Catalysis Today 442 (2024) 114919

Contents lists available at ScienceDirect

Catalysis Today

journal homepage: www.elsevier.com/locate/cattod

Reticulated porous structures of $La_{0.8}Al_{0.2}NiO_{3-\delta}$ perovskite for enhanced green hydrogen production by thermochemical water splitting

Alejandro Pérez [a], María Orfila [a], Elisa Díaz [a], María Linares [a], Raúl Sanz [a,b], Javier Marugán [a,b], Raúl Molina [a,*], Juan A. Botas [a,b]

[a] Chemical and Environmental Engineering Group, Universidad Rey Juan Carlos, C/ Tulipán s/n, Móstoles, Madrid 28933, Spain
[b] Instituto de Investigación de Tecnologías para la Sostenibilidad, Universidad Rey Juan Carlos, C/ Tulipán s/n, Móstoles, Madrid 28933, Spain

ARTICLE INFO

Keywords:
Perovskites
Thermochemical water splitting
Green hydrogen
Reticulated porous ceramic structure
Solar energy

ABSTRACT

The preparation and optimisation of $La_{0.8}Al_{0.2}NiO_{3-\delta}$ (LANi82) perovskite shaped as reticulated porous ceramic (RPC) structures for H_2 production by thermochemical water splitting is presented for the first time. The perovskite was first synthesised in powder form following a modified Pechini method. The redox properties of the LANi82 were first tested under N_2/air flow in a thermogravimetric analyser. After that, the sponge replica method for preparing RPCs was optimised in terms of slurry composition and final thermal treatment to obtain a LANi82-RPC structure with porosity and strength appropriate to enhance heat and mass transfer in further solar reactors. The optimised LANi82-RPC material showed an outstanding hydrogen production of 8.3 cm^3 STP/$g_{material}$·cycle at isothermal conditions (800 °C). This production was increased up to 11.5 cm^3 STP/$g_{material}$·cycle if the thermal reduction was performed at 1000 °C. Additionally, a stable activity with almost constant H_2 production in consecutive cycles was obtained for the optimised LANi82-RPC in both cases. The structure of the reticulated porous materials, with open macroporosity and wide interconnected channels, enhances heat and mass transfer, leading to higher hydrogen productions of the LANi82-RPC as compared to the materials as powder form in the same experimental set-up. These facts reinforce the favourable prospects of LANi82-RPC for large-scale hydrogen production, improving the coupling to current solar thermal concentration technologies developed, such as concentrated solar power tower.

1. Introduction

The impact of global climate change, due to greenhouse gases emissions [1], and the potential dependence on foreign energy of many countries as fossil fuels reserves are not distributed evenly worldwide, make it necessary to draw energy from renewable sources [2,3]. Electrification of some industrial and transportation sectors as well as certain residential applications, is not always technically possible. Consequently, the massive use of renewable sources to solve these problems is not feasible in the short to medium term. For that reason, one of the most important challenges for the world in the current decade is developing a clean and sustainable carbon-neutral fuel to help in the fight against the global energy crisis and environmental pollution [4,5].

In this context, hydrogen (H_2), as fuel, is considered the most promising alternative energy carrier due to its high energy density (120 MJ/kg) and the fact that its combustion product (H_2O) is environmentally friendly [3,6]. In 2019, Europe used 339 TWh (low heating value, LHV) of hydrogen per year, mainly as a feedstock to make other materials or to produce heat in industry, and the projection to 2050 is a growth in the contribution of hydrogen in Europe's energy mix for energy uses from the current < 2 % to more than 23 % (74 % of it for transport, power generation and buffering, heating and power for buildings and industry energy) [7–9]. This fact demonstrates that, in spite of the expectations around hydrogen as a key factor for the transition to a climate neutrality scenario, nowadays, the role of hydrogen as an energy vector is minimal. The main reasons are the lack of technological development for final use applications as well as the difference in cost as compared to other fuels, 1–1.5 €/kg fossil fuels as compared to 5–7 €/kg for renewable hydrogen coming from water electrolysis with renewable electricity [10]. Hydrogen can be obtained by breaking the chemical bonds of natural gas and light hydrocarbon compounds through processes such as steam reforming, partial oxidation, autothermal reforming or gasification, obtaining the so-called grey hydrogen, or blue hydrogen if carbon capture and storage techniques are

* Corresponding author.
E-mail address: raul.molina@urjc.es (R. Molina).

https://doi.org/10.1016/j.cattod.2024.114919
Received 31 January 2024; Received in revised form 18 June 2024; Accepted 25 June 2024
Available online 30 June 2024

applied for capturing the CO_2 produced in those processes [11,12]. However, the desirable hydrogen production should put together renewable energy and renewable sources, leading to the so-called green hydrogen. That is the case of the hydrogen obtained from: i) electrolysis of water using renewable energy as a source of electricity with zero CO_2 emissions, ii) biogas reforming, iii) biochemical conversion of biomass, only if sustainability requirements are met during the production process [12–14]. In this sense, the availability of solar energy (Earth is hit by 430 EJ per hour every day [15]) makes thermal water splitting using concentrated solar energy an attractive alternative for green hydrogen production [6]. Nevertheless, despite the simplicity of the process, the direct thermolysis of water requires a high amount of energy, and temperatures as high as 2500 °C to produce only 9 % of water dissociation (at 1 bar). These operational temperatures cannot be reached with the current solar thermal systems [16]. So, solar driven thermochemical cycles for water splitting have attracted attention as a potential and promising alternative for green hydrogen production [3,17]. In these processes, water can be dissociated into hydrogen and oxygen through different consecutive reactions with lower temperature requirements than thermolysis. Particularly, those thermochemical cycles based on metal oxides that follow a two-step mechanism: first, oxygen is released during the thermal reduction of the metal oxide (R1), being α the extent of reduction. After that, the reduced solid reacts with H_2O vapour, reoxidising the solid and producing hydrogen in a second step (R2). The result after the cycle is the generation of H_2 and O_2 by splitting the water molecule. However, this process has as an important drawback that the reduction temperature reaches values up to 1500 °C, depending on the metal oxide employed in the process [18,19].

$$Me_xO_y \rightarrow Me_xO_{y-\alpha} + \alpha/2\ O_2 \quad \text{(R1)}$$

$$Me_xO_{y-\alpha} + \alpha\ H_2O \rightarrow Me_xO_y + \alpha\ H_2 \quad \text{(R2)}$$

Among the large number of metal oxides reported in the literature for this application, ceria (CeO_2) is one of the most studied, mainly due to its thermodynamically favourable oxidation, good kinetics, and good thermal stability. However, ceria requires high reduction temperatures (close to 2000 °C) to achieve a full reduction extent [20]. To solve the problem, ceria can be partially reduced following a reaction close to R1, obtaining non-stoichiometric ceria using temperatures for thermal reduction close to 1500 °C [21–24]. However, this temperature is still too high, and the low hydrogen production under these conditions makes it necessary to find alternative materials for this application.

Considering the above-mentioned problems, it is mandatory to find new materials that can be thermally reduced at low temperatures (≤ 1000 °C) without decreasing the hydrogen production. In this context, non-stoichiometric oxides can be used for this application as they show an efficient reduction capacity at moderate temperatures, favourable oxidation thermodynamics, in both cases (reduction/oxidation) with fast kinetics, and with remarkable stability at high temperatures.

Perovskites are mixed oxides with ABO_3 or A_2BO_4 type structure, in which position A is occupied by a large cation (e.g. La or Sr), and B by a smaller metallic cation (e.g.: Mn, Fe, Co, Ni or Cu). Both sites A and B can be partially occupied simultaneously by different metallic cations with different oxidation states without modifying the crystalline structure of the perovskite matrix. The electroneutral state is consequently achieved by the formation of oxygen vacancies, leading to non-stoichiometry perovskites. These changes improve the redox activity of the perovskites due to the presence of oxygen vacancies and the multiple oxidation states of metal in -B position [16,25]. Perovskites have been proposed in multiple applications due to precisely their redox properties, such as heterogeneous redox catalysts or solid fuel cell electrocatalysts.

While basic research is commonly devoted to identifying redox pairs formulations with outstanding redox activity and long-term stability under concentrated solar irradiation [26,27], the development of solar reactors capable of performing the process with enhanced efficiency and scalability for further industrial application should be addressed. Among solar reactor concepts proposed to get temperatures high enough for the thermal reduction, reticulated porous ceramic (RPC) structures placed in a cavity-receiver have been proposed as a simple alternative promoting the pass of the solar irradiation into the reduction/oxidation space [28–32]. Combining a cavity-receiver with pure cerium oxide shaped as RPC, with two reactors working in parallel, allows a good volumetric radiative absorption with a high mass loading of active material in the reactor for the application [23].

Actually, RPC structures have been proposed as potential candidates for the design of thermochemical water splitting solar reactor, not only for ceria-based materials [33], but also for conforming other mixed metal oxides [34,35].

This work describes the preparation, evaluation, and optimisation of RPCs structures of $La_{0.8}Al_{0.2}NiO_{3-\delta}$ to be used for hydrogen production by two-step thermochemical water splitting. This perovskite has been proposed by the authors in a previous work with a remarkable production of 5.6 cm^3 STP $H_2/g_{material}$·cycle, working at reduction and oxidation temperatures of 1000 °C and 800 °C, respectively, and 4.4 cm^3 STP $H_2/g_{material}$·cycle under isothermal conditions at 800 °C, when it is used as powder shape [36]. In both cases, the reduction was performed using N_2 flow as inert gas and reoxidation with N_2 saturated with H_2O vapour.

In this work, the material was firstly prepared in powder following a modified Pechini method reported in the literature [36,37], and its redox capacity, activity and cyclability at 1000 and especially 800 °C was thoroughly evaluated during continuous step-by-step production of O_2 and H_2. Afterwards, the macroscopic shaping of the powder into an RPC structure following the replica method used for manufacturing ceramic sponges was optimised. The activity and cyclability of this RPC were analysed using the powder material as a reference. This is the first time that $La_{0.8}Al_{0.2}NiO_{3-\delta}$ in RPC structures working at a low temperature of 800 °C is reported, being a promising alternative for the development of clean and efficient H_2 production processes in the near future at higher TRL (technology readiness level) than current advances, which can be considered in the phase of "research to prove feasibility" (TRL 2–4) [38,39].

2. Materials and methods

2.1. Materials

Different metal nitrates were used for the synthesis of the $La_{0.8}Al_{0.2}NiO_{3-\delta}$ following the Pechini method: $La(NO_3)_3{\cdot}6H_2O$ (Honeywell, 99 % purity), $Al(NO_3)_3{\cdot}9H_2O$ (Panreac, 98 % purity), $Ni(NO_3)_2{\cdot}6H_2O$ (Fluka, 97 % purity). Contraspum KWE (anti-foaming agent), Dolapix CE 64 (deflocculating agent) and Optapix PA 4G (binder agent) were supplied by Zschimmer & Schwarz (Spain). Polyurethane foams (PUS, 40 ppi, pores per linear inch) were acquired at Comercial de Industria y Representaciones S.L. (CIR-62, Spain).

2.2. Preparation of $La_{0.8}Al_{0.2}NiO_{3-\delta}$ reticulated porous ceramic (RPC) structures

$La_{0.8}Al_{0.2}NiO_3$ (LANi82) was synthesised by a modified Pechini method following the procedure described elsewhere [36,40]. First, the metal nitrates were incorporated in the desired proportion into a citric acid solution and stirred at 70 °C for 10 min. The citric acid is used as chelating agent of the metallic species. Afterwards, ethylene glycol was added to produce a polymer with the metallic cations homogenously distributed and the new mix was stirred for 2 h at 90 °C. Ammonium hydroxide was added until a pH of 9 was reached, favouring the formation of stable metal citrate species, and preventing precipitation of individual hydroxides. After that, the solution was heated at 130 °C for 4 h to promote the polyesterification between the citrate and ethylene glycol, forming an extended covalent network with the metal ions

entrapped homogeneously. Finally, the gel was washed, filtered and dried overnight at 120 °C which allows to obtain a resin. The resin was milled using an agate mortar and the powder obtained was calcined for 6 h under static air at 1000 °C [36].

Several LANi82-RPC samples were prepared by optimising the replica method used for manufacturing ceramic sponges [41–44], and also used to prepare pure ceria and doped ceria RPCs in literature [23, 31]. The procedure is summarised in Fig. 1. Firstly, a slurry with the viscosity and consistency necessary for a good impregnation of the organic polymer used as scaffold should be prepared. $La_{0.8}Al_{0.2}NiO_{3-\delta}$ particles were dispersed in water (1:3 mass ratio) using the deflocculating agent to prevent agglomeration of the smaller particles during the process. The suspension was stirred at 85 °C for 15 min, before the addition of the organic binder agent. After that, the slurry was stirred for 30 more minutes, adding several drops of the non-ionic anti-foaming reagent. The proportions of the reactants and precursors were optimised, with the formation of a stable RPC structure (shaped structure) at the end of the overall process as response variable. The polyurethane foam (PUS) was shaped as a cylinder of 3 × 3 cm and submerged in the slurry, covering the surface of its walls with the slurry. The PUS was maintained in the slurry for 10 min, and then the excess of slurry was removed from surfaces and the cylinder dried at ambient temperature. The coating procedure was repeated twice, obtaining an appropriate density and thickness of the coated film to ensure the mechanical stability of the final RPC after the removal of the PUS.

The polyurethane foam acted as sacrificing organic scaffold, being calcined and burned out from the final structure. At the same time, the inorganic walls were sintered during this final calcination step. The heating rate and the final temperature are critical variables in the final porosity and mechanical strength of the RPC, and consequently, both were optimised by evaluating different calcination programs (Fig. S1).

2.3. Physicochemical characterisation of materials

The composition of the perovskite synthesised by the Pechini method was determined by inductively coupled plasma atomic emission (ICP-AES) analysis collected in a Varian Vista AX spectrometer. This technique allows obtaining the La/Al/Ni composition of the sample, being the oxygen content estimated from the mass balance. The morphology and crystalline structure of the materials were analysed by X-ray diffraction (XRD) with a Philips XPert diffractometer using CuKα radiation and Scanning Electron Microscopy (SEM), with a Philips Scanning Electron Microscope XL30 FEG with an accelerating voltage of 5.00 kV and a magnification of 60.0. Redox capacity of the perovskite with the temperature was evaluated by thermogravimetric analysis (TGA) in a TG/DSC equipment from Mettler Toledo. Thermal reduction was performed under continuous N_2 flow (100 mL/min), heating rate of 10 °C/min, starting from 45 °C up to 1000 °C. After that, oxidation was performed in air (100 mL/min) with a cooling rate of − 10 °C/min until reaching 45 °C again. The pore size distribution and the porosity of the LANi82-RPCs were determined by an AutoPore IV 9500 series equipment from Micromeritics, using the Washburn equation [45]. The mechanical strength of the LANi82-RPC structures was evaluated using a stepper motor powered test stand equipment, model TVO 500N500S, for compression force measurements. This equipment allows a precise adjustment of the transversal movement speed of the pressure disc (100 mm/min in this work). The measures were repeated in triplicate for each RPC, using RPC probes of cylindrical shape with a diameter of and length of ca. 3.5 cm and 3.2 cm, respectively.

2.4. Analysis of water splitting capability and hydrogen production efficiency of the LANi82-RPC structure under different thermal reduction conditions

The capability of the LANi82-RPC to produce hydrogen by thermochemical water splitting was tested using a high temperature tubular furnace (Nabertherm RHTH 70-600/18) coupled to two different gas analysers in order to quantify de amount of oxygen and hydrogen released in each step of the thermochemical cycle [46]. In a typical cycle, 14 g of LANi82 -RPC were placed into the tubular furnace as a packed bed (Fig. 2). The furnace was heated up to the final reduction temperature (800–1200 °C) at 10 °C/min under a continuous flow of 50 NL/h of nitrogen used as inert gas carrier (with a rating of 5.0, that is a 99.999 % purity). Once the oxygen was released from the material, the temperature was decreased down to the oxidation temperature (800 °C) or maintained if the reduction was performed at that temperature. Once reached the oxidation temperature, the nitrogen flow of 50 NL/h was saturated in water at 80 °C ($P_{H2O} = 7.2{\cdot}10^{-4}$ atm) before passing to the tubular furnace. This step promotes the reoxidation of the perovskite, releasing hydrogen, and closing the cycle. Once hydrogen is not detected in the outlet stream from the furnace, the temperature is raised up to the desired temperature again under continuous nitrogen flow free of water, at the same heating rate, starting a new cycle. Once finished the last cycle, the tubular furnace was cooled down to room temperature in order to open it, recovering the active metal oxide and finishing the process. It must be noted that the first cycle was discarded in all the cases as it is usually considered as an activation step. Actually, it is the only cycle in which reduction starts at room temperature, instead of

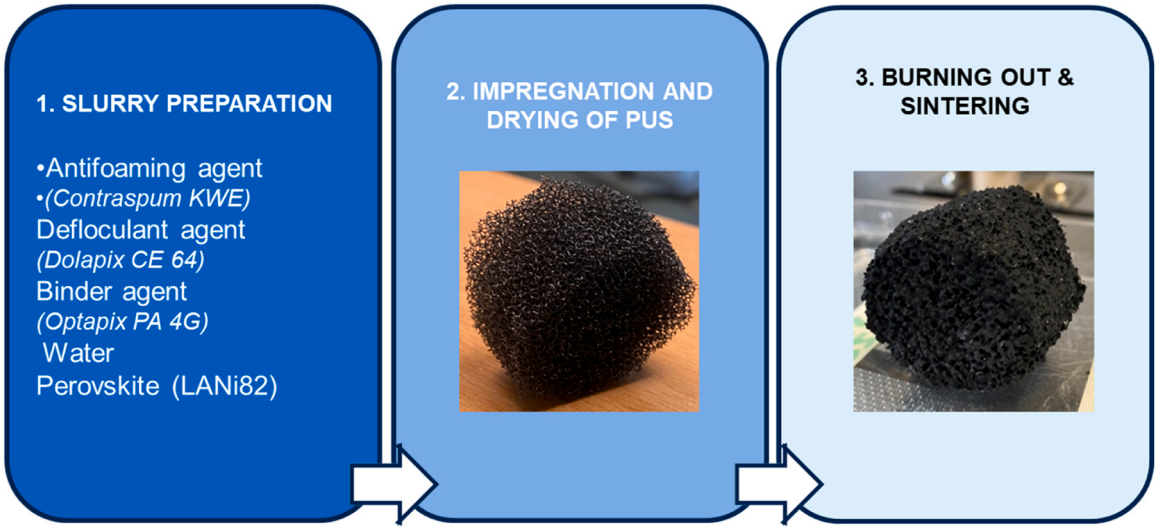

Fig. 1. Scheme of the preparation of LANi82 –RPCs by the replica method.

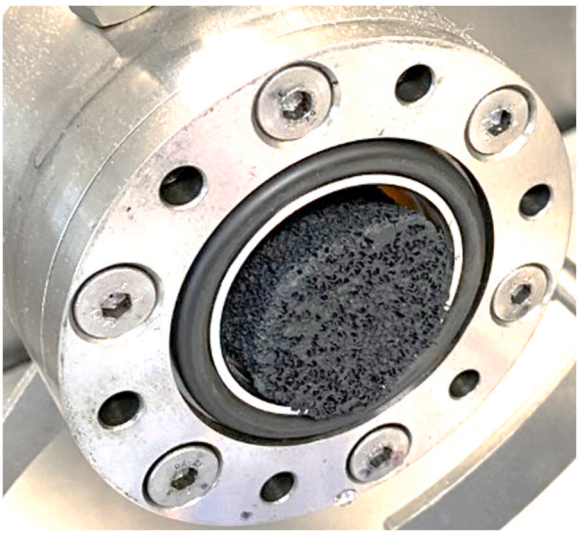

Fig. 2. Picture of the perovskite-based RPC structure inside the high temperature tubular furnace.

switching between reduction and oxidation temperature.

In both reactions (reduction and reoxidation), the outlet gas mixture stream passed through a cooler and a moisture trap to remove any trace of water prior quantification of the oxygen and hydrogen content using paramagnetic and thermal conductivity detectors, respectively (Xstream-XE analyser from Emerson Process Management GmbH & Co.). Both detectors were calibrated using nitrogen (the inert gas carrier) as zero gas and 0.5 % O_2/N_2 or 0.5 % H_2/N_2 streams as span, respectively. O_2 and H_2 detectors are located after the moisture trap and they are online and measuring simultaneously during both reaction steps, to discard leaks of air in the tubular furnace and the tubing during operation. The components of the gaseous stream coming from the tubular furnace in each step of the cycle were also monitored using a mass spectrometer, model OmniStar/ThermoStar GSD 350 from Pfeiffer Vacuum GmbH, with an atomic mass unit range of 1–100 a.m.u. This equipment was also connected online after the Emerson Xstream analyser, monitoring nitrogen, oxygen and hydrogen during the complete cycle and discarding the presence of other compounds.

In addition to the thermochemical cycles with the RPC structures, the LANi82 perovskite as powder was also tested in the tubular furnace under the same experimental protocol. In that case, 1 g of the material as powder was placed as a thin layer in a Pt/Rh crucible inside the tubular furnace, in order to identify any differences in performance between the perovskite placed in the reaction system as a reticulated porous structure and as a powder bed.

3. Results and discusion

3.1. Physicochemical characterisation of the powder perovskite

The LANi82 perovskite was first analysed by ICP-AES, XRD and SEM to confirm the properties previously determined when synthesising the perovskite following the modified Pechini method at basic pH [36]: atomic metallic composition close to the theoretical one (La/Al/Ni of 0.84/0.21/1, as compared to 0.8/0.2/1). The oxygen content was determined by weighing the difference between the total mass used for the ICP measurement and the amount of each metal presented in the perovskite. Afterwards, the difference between the theoretical one and the previously determined allows to estimate the non-stoichiometric oxygen ($\delta = -0.07$).

According to the XRD (Fig. S1) and the Rietveld analysis (Table S1), the material presents a single perovskite phase with a slightly distorted orthorhombic structure (space group *Pnma*-62), with a Goldschmidt tolerance factor (t) of 0.842 determined through the chemical composition of the perovskite and the atomic radius of the elements following Eq. (1). This value is in accordance with the reported in literature for perovskite with monoclinic or orthorhombic crystal structure ($t < 0.97$) [47]. Also, it must be noticed the absence of other peaks from impurities or other crystalline phases. SEM revealed a wide particle size distribution ranging from 25 to 100 μm.

$$t = \frac{r_A + r_O}{\sqrt{2}\cdot(r_B + r_O)} \quad (1)$$

3.2. Redox properties of the LANi82 perovskite

The redox capacity of the LANi82 was evaluated by TGA at a maximum temperature of 1000 °C (Fig. 3 and Table S2). Higher temperatures were not evaluated according to previous studies showing a lack of stability of this perovskite at higher temperatures [36]. After the first redox cycle, considered as a final thermal step for degassing and activating the material, thermal reduction starts at a temperature of ca. 600 °C, reaching values of ca. 0.13 % at 800 °C and ca. 0.45 % at the maximum temperature of 1000 °C. This reduction capacity of the material, even at 800 °C, is in agreement with previous results obtained by our group in a tubular furnace and reported in the literature [36].

Table S2 shows the values of weight gain and loss suffered by the material in each cycle. As it can be seen, there are small variations in the weight loss upon cycling, which can be related to thermal stability problems at 1000 °C.

3.3. Preparation and characterisation of LANi82 RPC structures

As shown in the previous sections, LANi82 is a promising material for large-scale hydrogen production through thermochemical cycles. In addition, thanks to the operating temperature, it can be coupled to current solar thermal devices, such as solar power towers, capable of reaching those temperatures [6,43]. However, in a potential future large-scale application, it is not possible to work with the material as synthesised in powder form, so its macroscopic shaping into a reticulated porous ceramic structure (RPC) was performed following the procedure described in the methodology section. In a first approach, the slurry and the calcination method were selected according to a previous work in which ceria mixed oxides RPC structures were prepared and tested for hydrogen production [23]. Thus a 0.83 wt% and 0.1 wt% of deflocculating agent and binder agent with respect to the perovskite powder were added to the mixture for the slurry preparation, and a calcination method consisting of heating the sample in air up to 1200 °C using a heating ramp of 2.5 °C/min, was selected. However, this

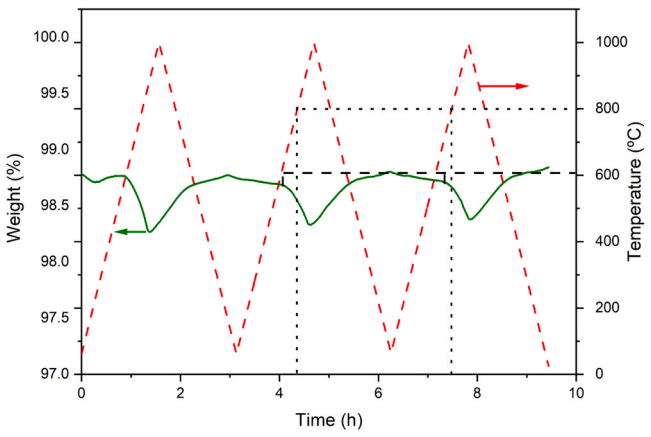

Fig. 3. TGA of LANi82 at maximum reduction temperatures of 1000 °C. Heating and cooling rate: ± 10 °C/min. Reduction in N_2 and oxidation in air flows (100 mL/min in both cases).

methodology produces a complete destruction of the LANi82-RPC structure, obtaining a coarse powder as a result of the process. The calcination stage is a compromise between the temperature necessary to remove the PUS from the final RPC structure (550–600 °C) [23], the temperature necessary for the final sintering of the perovskite particles that will form the walls of the RPC structure, and a heating ramp that allows the slow liberation of organics during the process, but avoiding structural damages or collapse of the RPC structure.

This step of the process was firstly optimised following a sequence of different heating ramps and final temperatures (Fig. S2), being the goal the formation of an RPC structure without partial collapsing of walls or complete destruction at the end of the process. According to that variable, the calcination method was finally optimised as described in Table 1.

However, the mechanical strength, porosity, and wall thickness, are critical variables for a further application of the RPCs and are also influenced by the slurry prepared in the first step of the process [29]. All those properties will affect the performance of the LANi82-RPC during the thermochemical cycles and the lifetime of the RPC when placed in a potential solar cavity reactor. Consequently, the influence of the composition of the slurry on the properties of the final RPC structure was also analysed by varying the proportion of deflocculating agent and organic binder during the slurry preparation (Table 2). It should be remarked that some compositions led to unstable structures that collapsed after calcination, even following the methodology proposed in Table 1. Those materials are identified in Table 2 as *shaped: No*, and they were not further considered nor characterised and evaluated for hydrogen production.

Once obtained four different RPC structures they have been observed by optical microscopy. The photographs are shown in Fig. 4.

As it can be seen the materials present random macro-channels of different sizes which are also randomly distributed along the RPC structures. Moreover, structures RPC-1 and -2 exhibited spots where the channel have partially collapsed, blocking them superficially.

One important variable related to the RPCs is the porosity of the final structure. For this reason, this variable has been measured by mercury porosimetry, and the results are shown in Fig. S3 (Supplementary information) and Table 3.

As it can be observed, the deflocculating and binder agents have a great influence on the porosity of the RPC structures. Deflocculating agent improves the dispersion of the perovskite particles in the slurry, promoting a more compact washcoat product. For that reason, the porosity increases from LANi82-RPC-1 to LANi82-RPC-2. At the same time, the binder agent is necessary to ensure the union among the powder particles in order to maintain the porous structure of the scaffold during the calcination process and thus avoid the collapse of the RPC. Thus, LANi82-RPC-3 and LANi82-RPC-4, with a higher amount of binder in the slurry composition, showed a higher porosity thanks to the better formation of the macroporous structure, even when increasing the amount of deflocculating agent in LANi82-RPC-3. Unfortunately, LANi82-RPC-5 has an insufficient amount of deflocculating agent, promoting the formation of a deficient coating of the sponge, leading to a collapse of the structure during calcination. Something similar occurs with LANi82-RPC-6 but, in this case, the low concentration of binder is not enough to attach and maintain the perovskite particles together as a uniform and continuous film over the sponge surface.

Table 1
Conditions of the optimised RPC calcination step.

Stage	Heating ramp (°C/min)	Isothermal stage (min)	Temperature (°C)
1	0.5	-	25–100
2	1.5	-	100–250
3	2.5	-	250–750
4	-	60	750
5	5	-	750–1000
6	-	400	1000

Table 2
Compositions of deflocculating and binder agents studied for shaping LANi82-RPCs.

Material	Deflocculant (wt%)*	Binder (wt%)*	Shaped
LANi82-RPC-1	1.67	0.10	Yes
LANi82-RPC-2	0.83	0.10	Yes
LANi82-RPC-3	1.67	0.20	Yes
LANi82-RPC-4	0.83	0.20	Yes
LANi82-RPC-5	0.41	0.10	No
LANi82-RPC-6	0.83	0.05	No

* (wt%) respect $La_{0.8}Al_{0.2}NiO_{3-\delta}$ powder in the mixture.

Additionally, another important fact is the total intrusion volume, which is the amount of Hg introduced into the RPC pores. As it can be seen, LANi82-RPC-1 showed the lowest intrusion volume, directly related to its lower porosity and total pore area, together with an increase in the density of the macroscopic structure. On the contrary, LANi82-RPC-3 showed the opposite behaviour, with the highest intrusion volume due to its highest porosity and total pore area and its lowest bulk density. Meanwhile, LANi82-RPC-2 and LANi82-RPC-4 showed intermediate characteristics.

Additionally, regarding the pore size distribution (Fig. S3), it can be seen that the RPCs that showed the highest porosity (RPC-3 and 4) are the ones that show a unimodal pore size distribution centred in 350 nm for RPC-3 and 400 nm for RPC-4. However, in the case of RPC-1 and 2 they show bimodal pore size distributions with pores with a diameter lower than 10 nm and pores of 200 nm (RPC-1) and 900 nm (RPC-2). This different behaviour could be explained by a partial collapse of the structure or the partial plugging of some of the pores and channels.

In any case, SEM micrographs (Fig. 5) show that the walls of the channels of the RPCs exhibit an irregular structure, with a high number of macro-pores and meso-pores of different sizes. Although this is particularly noticeable in samples RPC-3 and RPC-4, which have the highest total porosity, it is also clearly visible in structures RPC-1 and RPC-2. These meso- and macro- porosity have a high contribution to the total porosity, as it is shown in Table 3.

Another important value regarding the RPC structures is their mechanical strength. The mechanical strength was evaluated with the breaking strength of the different RPC materials synthesised. The results can be observed in Table 4, where a clear trend between average strength and porosity is observed (the higher the porosity, the lower the mechanical strength), although, considering the confidence interval in each RPC, the differences are almost negligible. Nevertheless, the porous structure of the open channel walls shown in Fig. 5 for all the samples, together with the high dimensions of these channels, could be responsible for the similar and low hardness of the structures.

3.4. Hydrogen production and cyclability with LANi82 RPC structures

The activity of the four RPC structures for hydrogen production was evaluated in the experimental set-up described previously. As an example, Fig. 6 shows the total O_2, H_2 and H_2/O_2 molar ratio, and the oxygen and hydrogen profiles evolved from the reactor obtained when the tests were performed with the LANi82 in powder form (Figs. 6a and 6c) while the results obtained with RPC-3 are shown in Figs. 6b and 6d. The integration of the area under the curves (Figs. 6c and 6d) allows to calculate the total amount of oxygen and hydrogen obtained in each cycle (Figs. 6a and 6b).

The results obtained for oxygen and hydrogen production in the five consecutive cycles tested for RPC-1 to RPC-4 are collected in Fig. 7. All the structures showed stable behaviour during the five consecutive cycles, accompanied by remarkable values of hydrogen production. However, it is important to note that the LANi82-RPC with the highest hydrogen production ($8.3 \pm 0.03\ cm^3\ STP/g_{material}{\cdot}cycle$) was the LANi82-RPC-3 followed closely by LANi82-RPC-4 with a value near to

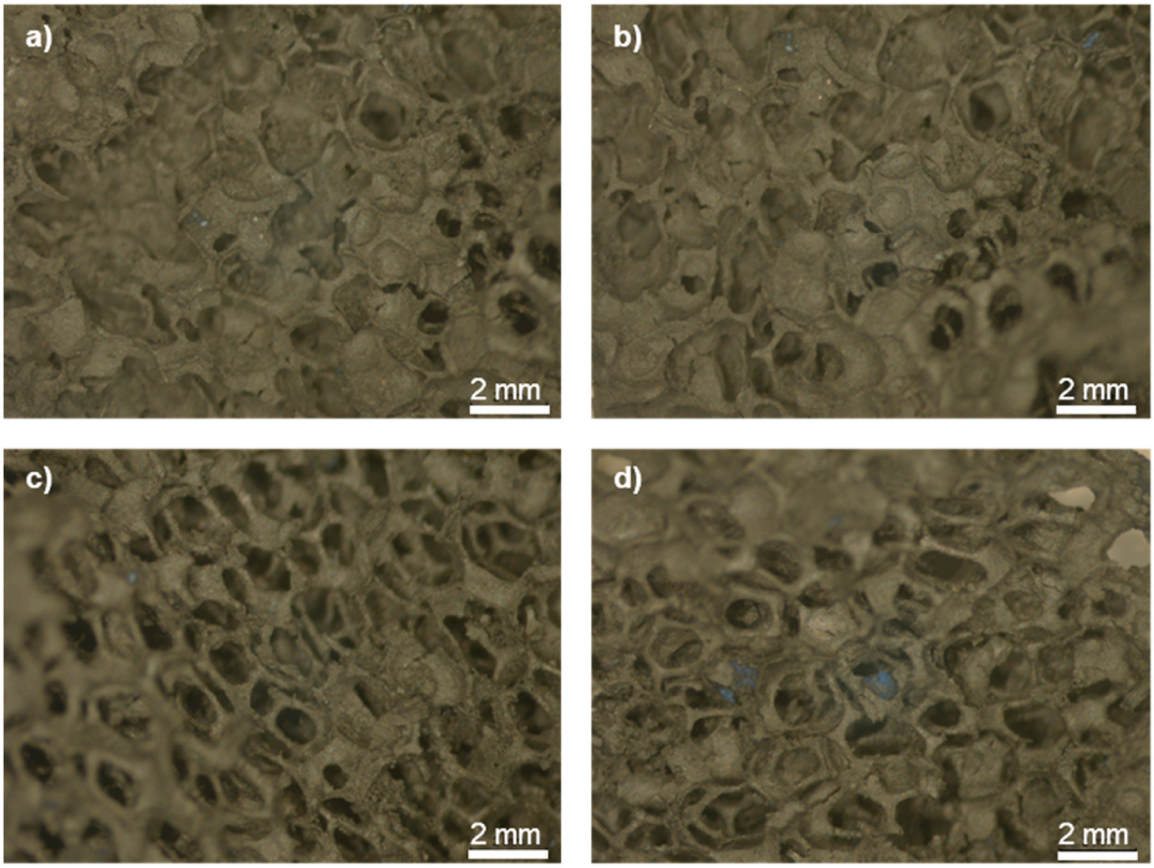

Fig. 4. Optical microscope photographs of the LANi82 structures: a) LANi82-RPC-1, b) LANi82-RPC-2, c) LANi82-RPC-3 and d) LANi82-RPC-4.

Table 3
Results of the mercury porosimetry.

Material	Total intrusion volume (mL/g)	Total porosity (%)	Meso- and macro-porosity (%)	Total pore area (m^2/g)
LANi82-RPC-1	0.23	48.31	32.3	1.14
LANi82-RPC-2	0.36	59.61	30.7	1.65
LANi82-RPC-3	0.39	65.39	32.6	1.70
LANi82-RPC-4	0.35	63.42	31.6	1.67

7.9 ± 0.13 cm^3 STP/ $g_{material}$·cycle. The better performance of these two structures could be due to their better properties in terms of porosity (65.39 and 63.42 %, respectively). Both LANi82-RPC-3 and LANi82-RPC-4 were prepared with higher binder proportion than the other, ensuring a better cohesion within the particles or perovskite in the RPC walls. Consequently, the materials with lower porosity showed the lowest hydrogen production, with 7.1 ± 0.04 and 6.7 ± 0.27 cm^3 STP/ $g_{material}$·cycle for LANi82-RPC-1 and LANi82-RPC-2, respectively.

One important fact is that the RPC structures outperformed the hydrogen production of the powder perovskite (4.4 ± 0.026 cm^3 STP/ $g_{material}$·cycle) by a factor of up to 1.5–2 [33]. A clear reason for this enhanced activity is due to the open macroporosity of the RPCs, improving the better contact and the diffusion of reactants and products as well as the heat transmission phenomena inside the tubular reactor.

Additionally, all the materials showed H_2/O_2 ratios close to 2 (Table 5), the theoretical stoichiometric one for water splitting.

The oxygen and hydrogen production under isothermal conditions (800 °C) using the LANi82-RPCs structures were confirmed by the results obtained in the mass spectrometer coupled to the outlet stream of the gas analysers (based on paramagnetic properties and thermal conductivity). Thus, only nitrogen (gas carrier) and oxygen were detected during reduction step, whereas only nitrogen and hydrogen were detected during hydrolysis. A comparative example of the signals obtained in the gas analysers and the mass spectrometer is shown in Fig. S4.

It should be remarked that, according to the water saturation condition of the carrier gas during the oxidation step, and the hydrogen produced in each cycle, the maximum water conversion (obtained with LANi82-RPC-3) was 23.1 %. This remarkable excess in water during the oxidation is necessary in order to run the cycle under isothermal conditions. It has been recently demonstrated that as the thermochemical cycle involves two consecutive reactions in an open system, isothermal operation is possible by ensuring the high partial pressure of water during the oxidation reaction and the low partial pressure of oxygen while the redox material is reduced [48]. To do that, not only oxygen, unreacted water and hydrogen are continuously removed from the system, but also an excess of water vapour:hydrogen ratio is necessary ($n_{hydrogen}$:$n_{water\ vapour} << 1$) in order to regenerate the redox material.

Once the activity of the LANi82-RPCs samples was evaluated, the materials were characterised by XRD. The analysis of the materials by XRD after five consecutive cycles at 800 °C (Fig. 8) showed that the perovskite materials do not present any structural modifications or segregation phenomena maintaining their initial phases.

These results reinforce the favourable prospects for large-scale hydrogen production by thermochemical cycles using the LANi82-RPC-3 or LANi82-RPC-4 materials at low temperatures (800 °C).

LANi82-RPC-3 was selected to evaluate hydrogen production in thermochemical water splitting performed at higher temperatures

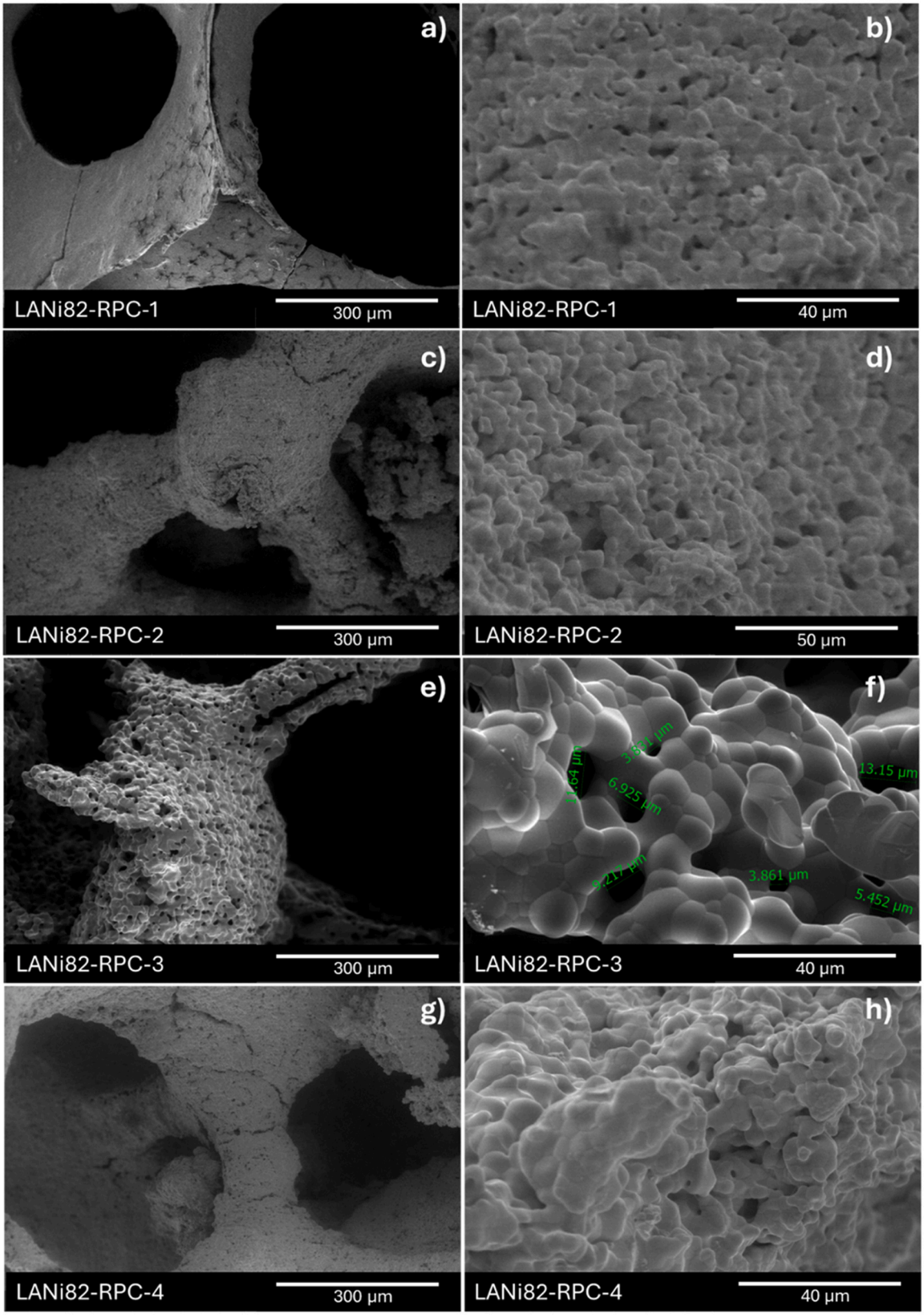

Fig. 5. SEM micrographs of the LANi82-RPC structures.

Table 4
Breaking strength of LANi82-RPC structures.

Material	Stress (kPa)
LANi82-RPC-1	3.86 ± 0.52
LANi82-RPC-2	3.74 ± 0.46
LANi82-RPC-3	3.65 ± 0.40
LANi82-PRC-4	3.70 ±0.77

(1000–1200 °C) during thermal reduction. The results are shown in Fig. 9, as well as those obtained at 800 °C with this RPC for comparison.

Increasing the reduction temperature from 800 to 1000 °C allows an increase in the hydrogen production from 8.3 ± 0.03 cm^3 STP/$g_{material}$·cycle to 11.3 ± 0.13 cm^3 STP/$g_{material}$·cycle, maintaining a stable behaviour during the 6 cycles. This is a remarkable enhancement of the hydrogen productivity although less than that expected according to the results obtained in the TG analysis (as the oxygen released during the reduction step in the tubular furnace is equivalent to 0.1 % of the mass of the RPC introduced in the tubular furnace at the beginning of the step, whereas 0.38 % mass variation was experimentally obtained in the TG; Fig. 2 and Table S2) due to the difference between reoxidation with air or based on the hydrolysis with vapour. O_2 and H_2 profiles of thermochemical cycles at 800 °C show a stable behaviour during the cycles (Fig. 10 a and b), with 70 min required for thermal reduction and hydrolysis taking ca. 60 min.

In the case of reduction at 1000 °C, the O_2 and H_2 profiles show the presence of two different oxygen sites as both graphs (Fig. 10 c and d) show two different zones in both steps of the cycles. Anyway, the time required for reduction and hydrolysis is 90 min in each case. Thus, the time required for a complete cycle is ca. 130 min and 180 min at 800 and 1000 °C, respectively, and the hydrogen production rate can be calculated as 0.0640 and 0.0635 cm^3 STP/$g_{material}$·min. This result is quite similar in both cases, marking the isothermal thermochemical water splitting at 800 °C as the best conditions for hydrogen production by thermochemical water splitting with the LANi82-RPC structure. Finally, both the hydrogen production and the O_2 and H_2 profiles (Fig. 10 e and f) show that the LANi82-RPC is non-stable in subsequent cycles with thermal reduction at 1200 °C, as shown previously in literature with this type of perovskite as powder, probably due to the presence of segregated phases and sintering phenomena [36]. Consequently, the hydrogen production decreases in each cycle, and the H_2/O_2 ratio drops below 2, as the reduced material cannot be completely reoxidised during the second step of each cycle, lowering the hydrogen production as compared to the previous one (Fig. 9).

In order to compare the results obtained in this study with other metal oxides shaped as macroscopic structures, reported in the literature, Table 6 summarises their hydrogen production and the reduction/oxidation conditions.

As it can be seen in Table 6, the $La_{0.8}Al_{0.2}NiO_{3-\delta}$ -RPC evaluated in this study showed similar or even higher results than other materials reported in the literature but working at lower temperatures, which implies higher solar efficiency and lower radiation losses in the

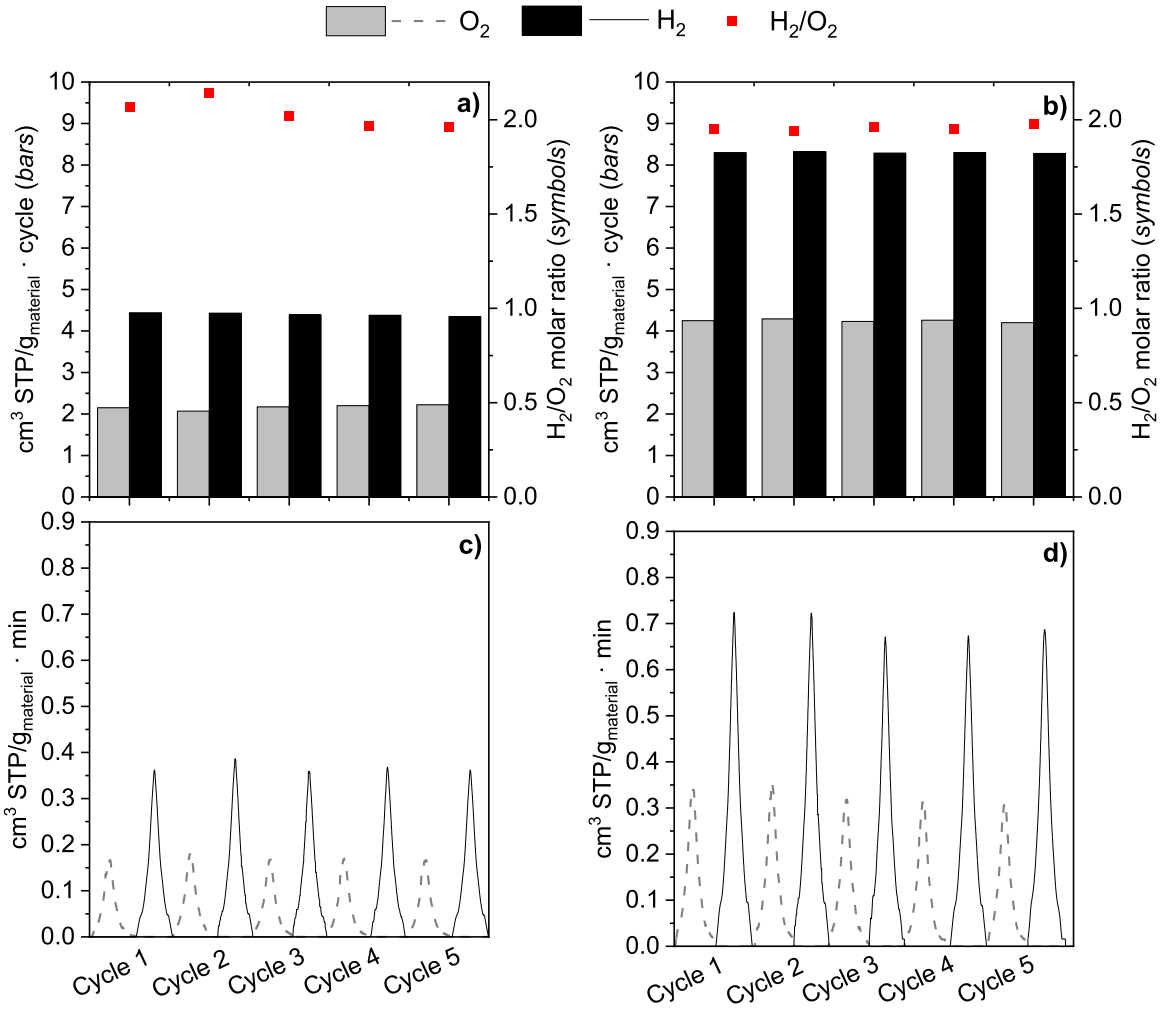

Fig. 6. O_2 and H_2 production profiles during thermochemical water splitting with LANi82 in powder form (a and c) and RPC-3 (b and d), under isothermal conditions at 800 °C.

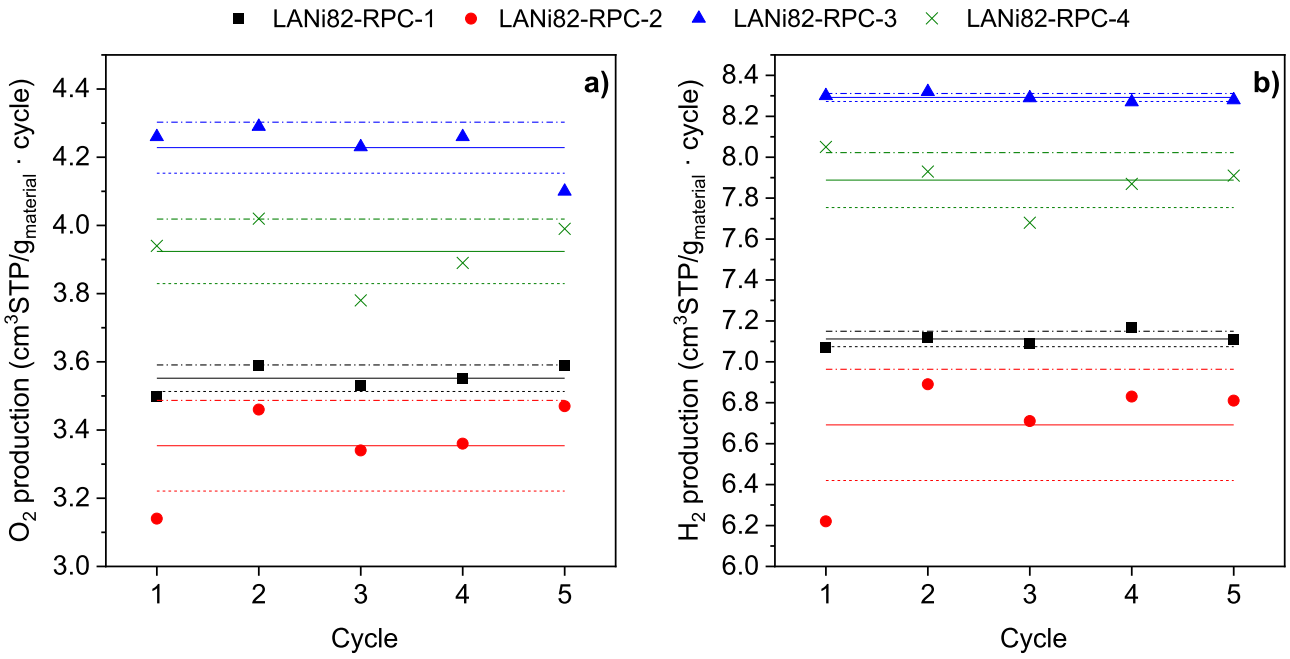

Fig. 7. a) O_2 and b) H_2 production during thermochemical water splitting with the LANi82-RPCs, under isothermal conditions of 800 °C (thermal reduction and hydrolysis). Straight lines are the average value, dash lines are the lower deviations, and dash-dot lines are the upper deviations.

Table 5
H_2/O_2 molar ratios during thermochemical cycles with the LANi82-RPCs.

Material	Cycle 1	Cycle 2	Cycle 3	Cycle 4	Cycle 5
LANi82-RPC-1	2.02	1.98	2.01	2.02	1.98
LANi82-RPC-2	1.98	1.99	2.01	2.03	1.96
LANi82-RPC-3	1.95	1.94	1.96	1.94	1.95
LANi82-RPC-4	2.04	1.97	2.03	2.02	1.98

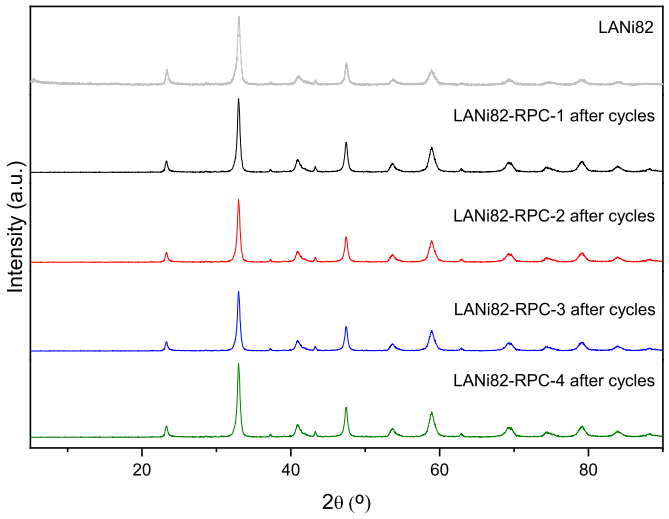

Fig. 8. XRD patterns for the LANi82-RPCs after the five consecutive cycles tested.

concentrated solar power facilities necessary to reach the operation temperatures.

The RPC structures were characterised by XRD and SEM after cycles at thermal reduction of 800–1200 °C. The XRD profiles are shown in Fig. 11 where the doted lines correspond to initial orthorhombic perovskite phase. As it can be seen, when the reduction was performed at 1200 °C new signals appeared indicating the presence of segregated

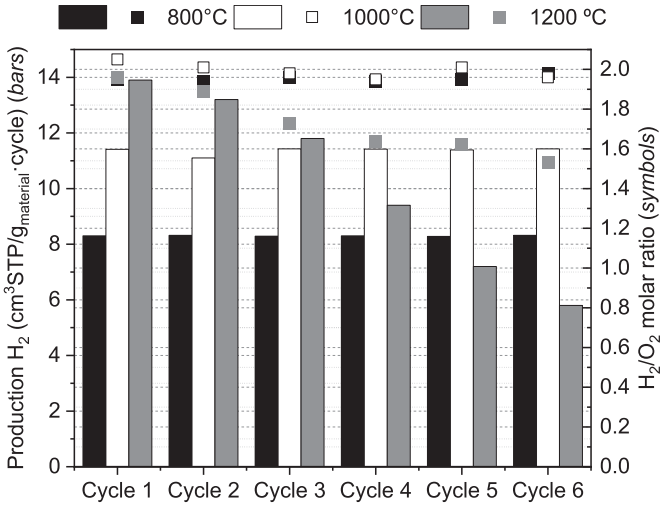

Fig. 9. H_2 production (bar graph) and H_2/O_2 molar ratio (square symbol) in 6 consecutive thermochemical cycles performed at reduction temperatures of 1200 °C (grey), 1000 °C (white) and 800 °C (black) and hydrolysis (reoxidation) of 800 °C.

phases from the main perovskite structure. This result is in accordance with the continuously decrease in the activity observed (Fig. 9) and the changes in the oxygen and hydrogen production profiles (Fig. 10 e and f). The XRD pattern of the RPC after thermochemical cycles at thermal reduction of 1000 °C is slightly different form the initial structure, which indicates that with a higher number of cycles the activity could decrease which is in accordance with results reported in literature [36]. All the signals identified in the XRD patterns are summarised in Table 7. As it can be seen these new signals are mainly due to different LaNiO perovskites, aluminium oxide, and aluminium and nickel mixed oxides. Finally, regarding the XRD pattern of the material tested isothermally at 800 °C it can be seen that new signals did not appear confirming its stability.

Regarding the SEM micrographs (Fig. 12), it can be seen that only

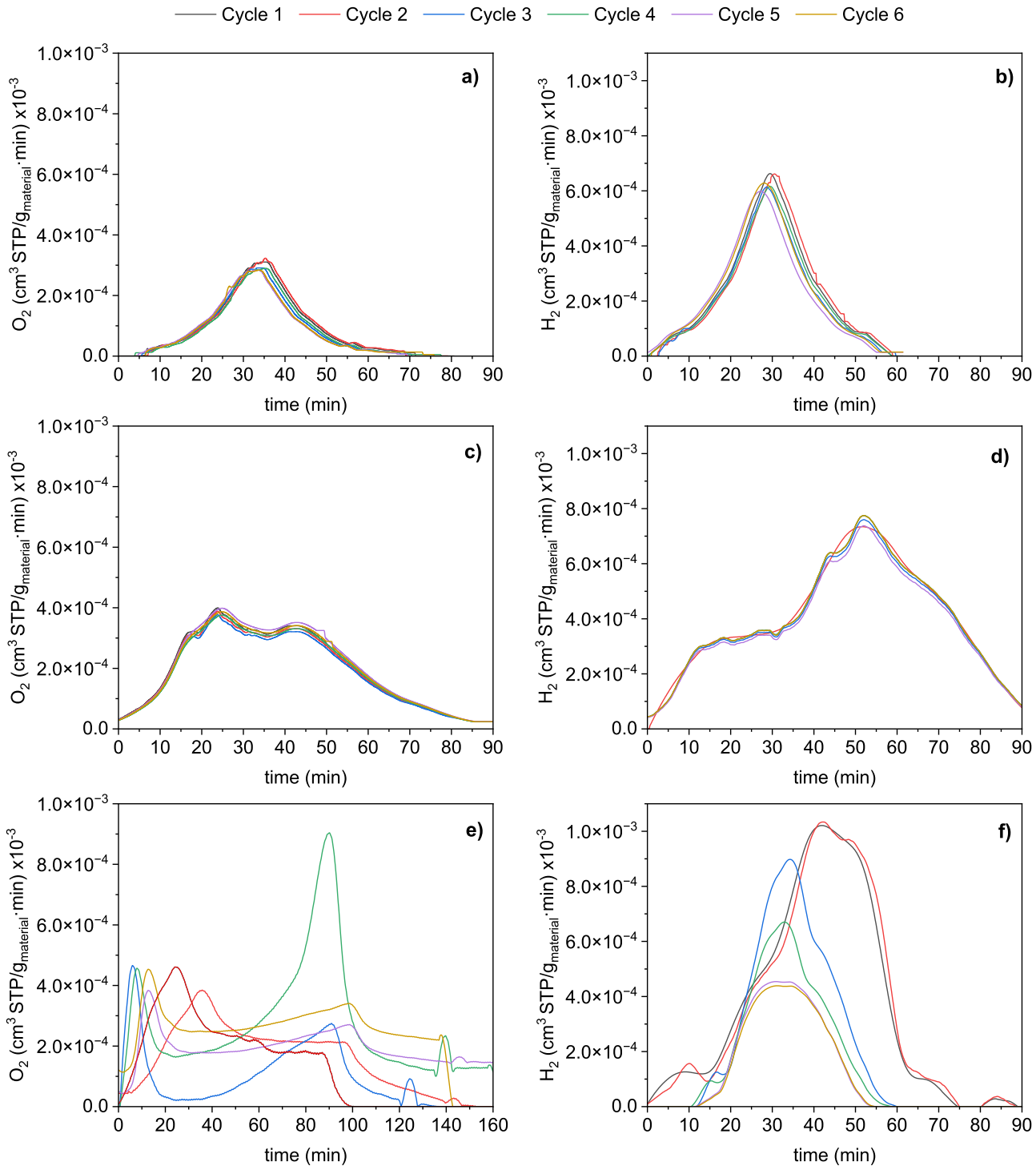

Fig. 10. Oxygen production profiles in 6 consecutive cycles at $T_{reduction}$ = 800 °C (a), $T_{reduction}$ = 1000 °C (c) and $T_{reduction}$ = 1200 °C (e), and corresponding hydrogen production profile at $T_{hydrolysis}$ = 800 °C (b, d and f, respectively).

new phases were observed when the material was tested at 1000 and 1200 °C (Fig. 12c–d), with particles corresponding to an oxide with a higher amount of aluminium according to the EDX analysis (Table S3). These results are in agreement with the activity tests and the XRD profiles and suggest that the RPC structure could be not stable at higher number of cycles performed at reduction temperatures higher than 800 °C.

4. Conclusions

This work shows the optimisation of the slurry composition for the washcoat process and calcination rates for the macroscopic shaping of perovskites as reticulated porous ceramic (RPC) structures showing how these parameters have a critical role in the final properties of the structures. Among all the LANi82-RPCs evaluated, the best one showed a hydrogen production of 8.3 cm^3 STP/$g_{material}$·cycle (almost double the value shown in literature with the perovskite as powder) with stable behaviour during the cycles tested. This improvement can be attributed

Table 6
Comparison of hydrogen production and experimental conditions of different metal oxides evaluated in thermochemical cycles.

Material	Reduction conditions	Hydrolysis conditions	H_2 (cm^3STP/g)	Ref.
RPC structures				
$Ce_{0.9}Fe_{0.1}O_2$	N_2 flow (99.999 %), 50 L/h; T: 1300 °C	H_2O/N_2 humidity: 100 % (at 1 atm and 80 °C); T: 800 °C	14	[23]
CeO_2	Ar flow (99.996 %); T: 1450–1600 °C	H_2O/N_2 humidity: 100 % (at 1 atm and 200 °C) T: 700–1200 °C	9	[33]
$(La_{0.65}Sr_{0.35})_{0.95}MnO_3$	Ar flow (99.999 %); T: 1400 °C	H_2O/Ar humidity: 100 % (at 1 atm and 200 °C); T: 1400 °C	4.47	[34]
$La_{0.5}Sr_{0.5}Mn_{0.9}Mg_{0.1}O_3$+ CeO_2	Ar flow (99.999 %), 0.2 NL/min; T: 1399 °C	Gas flow: 1.45 NL/min, H_2O/Ar: 0.25 T: 1040–671 °C	3.64	[35]
$La_{0.5}Sr_{0.5}Mn_{0.9}Mg_{0.1}O_3$+ CeO_2	Ar flow (99.999 %), 0.2 NL/min; T: 1409 °C	Gas flow: 3.30 NL/min, H_2O/Ar: 0.8 T: 1034–781 °C	5.72	[35]
$La_{0.5}Sr_{0.5}Mn_{0.9}Mg_{0.1}O_3$+ CeO_2	Ar flow (99.999 %), 0.2 NL/min; T: 1407 °C	Gas flow: 1.60 NL/min, H_2O/Ar: 0.8 T: 959–615 °C	4.1	[35]
$La_{0.8}Al_{0.2}NiO_{3-\delta}$	N_2 flow (99.999 %), 50 L/h; T: 800 °C	H_2O/N_2 humidity: 100 % (at 1 atm and 80 °C); T: 800 °C	8.3	This study
$La_{0.8}Al_{0.2}NiO_{3-\delta}$	N_2 flow (99.999 %), 50 L/h; T: 1000 °C	H_2O/N_2 humidity: 100 % (at 1 atm and 80 °C); T: 800 °C	11.5	This study
Fixed bed based on fibrous pellets				
CeO_2	Ar flow (99.999 %), 0.2 L/h; T: 1400 °C	H_2O/Ar humidity: 100 % (at 0.5 atm and 100 °C); T: 1050 °C	3.1	[49]

to the high porosity (65.39 %) of the RPC structure, improving heat and mass transfer processes.

Additionally, it has been demonstrated that this material can be thermally reduced at a temperature as low as 800 °C, much lower than the values reported in the literature for the metal oxides commonly studied which makes it possible to integrate the macroscopic structures in solar reactors with concentrated solar power technologies currently available such as solar power towers or parabolic dishes. Most important is the fact that this material can work isothermally, increasing the efficiency of the process as it deletes the cooling step between the reduction and oxidation reactions, maximising hydrogen production per cycle.

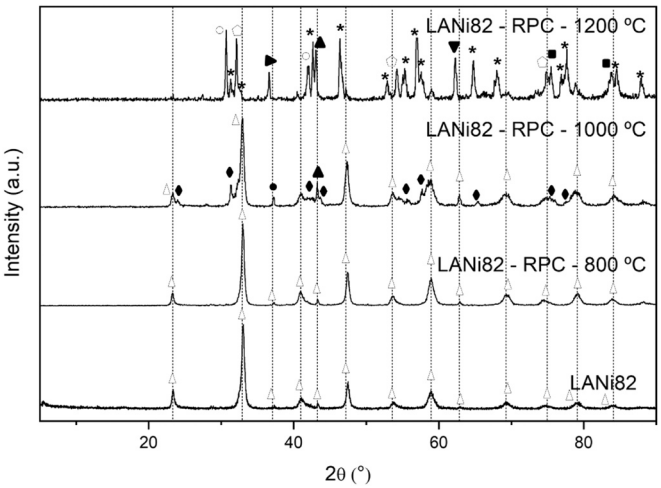

Fig. 11. XRD patterns for the LANi82-RPCs after the six consecutive cycles tested at different reduction temperatures.

Table 7
Signals identification in XRD patterns of the samples evaluated at different operation temperatures.

Symbol	Compound	Crystal system	Space group	Ref.
◆	$La_2NiO_{4.126}$	Tetragonal	*I4/mmm* (139)	COD 1533563
●	$Al_{2.4}O_4Ni_{0.3}$	Cubic	*Fd-3m*:2 (227)	COD 1535762
▲	Al_2O_3	Hexagonal	*R-3c*:4 (167)	COD 5000092
*	La_2NiO_4	Orthorhombic	*Cmca* (-*a*,*c*,*b*) (64)	COD 1540177
■	La_2NiO_4	Tetragonal	*I4/mmm* (139)	COD 1522571
⌂	$La_2NiO_{3.99}$	Tetragonal	*I4/mmm* (139)	COD 1533567
○	$Al_{11}LaNiO_{19}$	Monoclinic	*P63mmc* (194)	COD 1001680
▼	Al_2O_3	Hexagonal	*R-3c*:4 (167)	COD 9008081
►	Al_2NiO_4	Cubic	*Fd3m* (227)	ISCD 608815
Δ	$La_{0.8}Al_{0.2}NiO_3$	Orthorhombic	*Pnma* (62)	MP 22590

CRediT authorship contribution statement

Orfila María: Writing – review & editing, Methodology, Investigation, Data curation, Conceptualization. **Pérez Alejandro:** Writing – original draft, Methodology, Investigation, Data curation. **Sanz Raúl:** Writing – review & editing, Supervision, Methodology, Funding acquisition, Conceptualization. **Linares María:** Writing – review & editing, Validation, Methodology, Conceptualization. **Díaz Elisa:** Writing – original draft, Investigation, Data curation. **Botas Juan Angel:** Writing – review & editing, Validation, Supervision, Project administration, Methodology, Funding acquisition, Conceptualization. **Raul Molina:** Writing – review & editing, Supervision, Project administration, Methodology, Funding acquisition, Data curation, Conceptualization. **Marugán Javier:** Writing – review & editing, Methodology, Formal analysis, Conceptualization.

Declaration of Competing Interest

The authors declare that they have no known competing financial interests or personal relationships that could have appeared to influence the work reported in this paper.

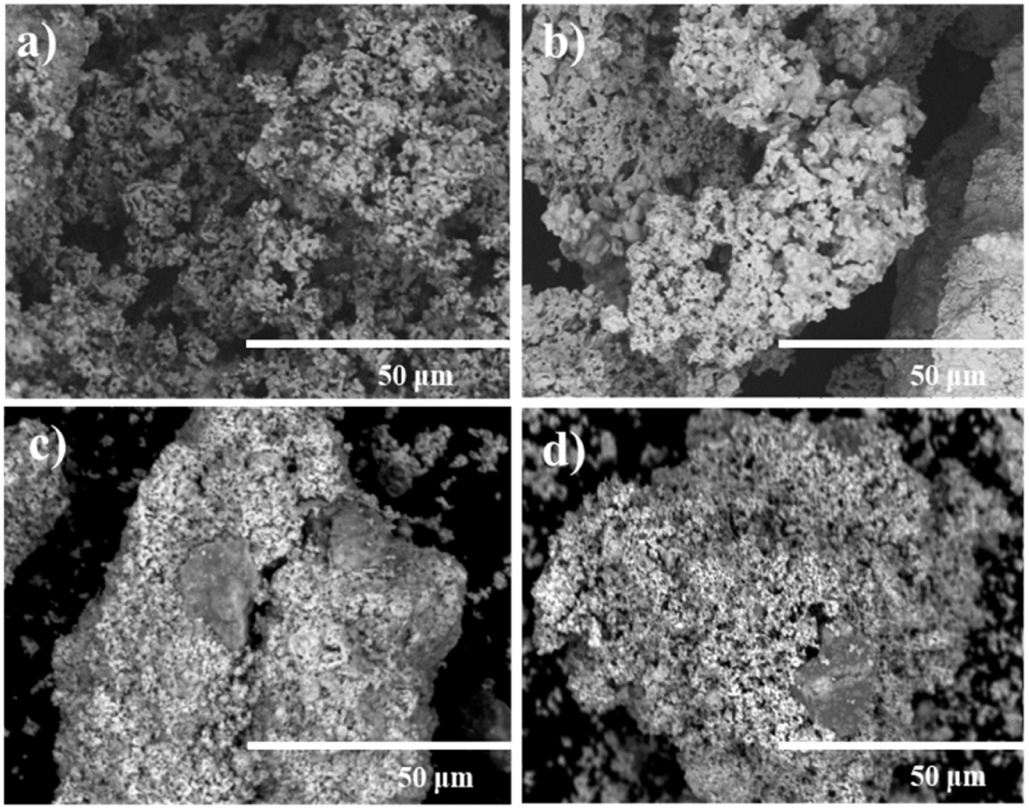

Fig. 12. SEM backscattering micrographs of the walls of the RPCs: a) raw material, and after the cycles performed at b) reduction temperature = 800 °C, c) reduction temperature = 1000 °C and d) reduction temperature = 1200 °C.

Data availability

Data will be made available on request.

Acknowledgments

The authors thank “Comunidad de Madrid” and European Structural Funds for their financial support to ACES2030-CM project (S2018/EMT-4319), SOLTOCOMB (M-2174) and ONEHYDRO (M-2733) URJC projects. This work is part of the project TED2021-132540B-I00, funded by MCIN/AEI/10.13039/501100011033 and by the European Union "NextGenerationEU"/PRTR. The authors also want to thank Zschimmer &Schwarz España S.A. for supplying Optapix PA 4G, Dolapix CE 64 and Contraspum KWE, for the RPC preparation.

Appendix A. Supporting information

Supplementary data associated with this article can be found in the online version at doi:10.1016/j.cattod.2024.114919.

References

[1] M.F. Vostakola, B.A. Horri, Progress in material development for low-temperature solid oxide fuel cells: a review, Energies 14 (2021), https://doi.org/10.3390/en14051280.
[2] P. Nikolaidis, A. Poullikkas, A comparative overview of hydrogen production processes, Renew. Sustain Energy Rev. 67 (2017) 597–611, https://doi.org/10.1016/j.rser.2016.09.044.
[3] I. Dincer, C. Acar, Review and evaluation of hydrogen production methods for better sustainability, Int. J. Hydrog. Energy 40 (2014) 11094–11111, https://doi.org/10.1016/j.ijhydene.2014.12.035.
[4] J.O. Abe, A.P.I. Popoola, E. Ajenifuja, O.M. Popoola, Hydrogen energy, economy and storage: review and recommendation, Int. J. Hydrog. Energy 44 (2019) 15072–15086, https://doi.org/10.1016/j.ijhydene.2019.04.068.
[5] A. Midilli, M. Ay, I. Dincer, M.A. Rosen, On hydrogen and hydrogen energy strategies I: current status and needs, Renew. Sustain. Energy Rev. 9 (2005) 255–271, https://doi.org/10.1016/j.rser.2004.05.003.
[6] A.J. Carrillo, J. González-Aguilar, M. Romero, J.M. Coronado, Solar energy on demand: a review on high temperature thermochemical heat storage systems and materials, Chem. Rev. 119 (2019) 4777–4816, https://doi.org/10.1021/acs.chemrev.8b00315.
[7] E. Comission, Communication from the Commission to the European Parliament, the Council, the European Economic and Social Committee and the Committee of the Regions: a hydrogen strategy for a climate-neutral Europe, COM, 2020, 301. 2020.
[8] J.R. Centre, Hydrogen use in EU decarbonization scenarios, 2019, 2019.
[9] F.C. Undertaking, H. 2 J, Hydrogen Roadmap Europe: A Sustainable Pathway for the European Energy Transition, Publications Office, 2019. ⟨https://doi.org/10.2843/341510⟩.
[10] D.J. Jovan, G. Dolanc, Can green hydrogen production be economically viable under current market conditions, Energies 13 (2020), https://doi.org/10.3390/en13246599.
[11] A. Ajanovic, M. Sayer, R. Haas, The economics and the environmental benignity of different colors of hydrogen, Int. J. Hydrog. Energy 47 (2022) 24136–24154, https://doi.org/10.1016/j.ijhydene.2022.02.094.
[12] F. Zhang, P. Zhao, M. Niu, J. Maddy, The survey of key technologies in hydrogen energy storage, Int. J. Hydrog. Energy 41 (2016) 14535–14552, https://doi.org/10.1016/j.ijhydene.2016.05.293.
[13] F. Safari, I. Dincer, A review and comparative evaluation of thermochemical water splitting cycles for hydrogen production, Energy Convers. Manag. 205 (2020) 112182, https://doi.org/10.1016/j.enconman.2019.112182.
[14] T. da Silva Veras, T.S. Mozer, D. da Costa Rubim Messeder dos Santos, A. da Silva César, Hydrogen: trends, production and characterization of the main process worldwide, Int. J. Hydrog. Energy 42 (2017) 2018–2033, https://doi.org/10.1016/j.ijhydene.2016.08.219.
[15] N.S. Lewis, D.G. Nocera, Powering the planet: chemical challenges in solar energy utilization, Proc. Natl. Acad. Sci. USA 103 (2006) 15729–15735, https://doi.org/10.1073/pnas.0603395103.
[16] M. Orfila, M. Linares, R. Molina, J.A. Botas, J. Marugán, R. Sanz, Thermochemical hydrogen production using manganese cobalt spinels as redox materials, Int. J. Hydrog. Energy 42 (2017) 13532–13543, https://doi.org/10.1016/j.ijhydene.2017.02.027.
[17] V.K. Budama, N.G. Johnson, A. McDaniel, I. Ermanoski, E.B. Stechel, Thermodynamic development and design of a concentrating solar thermochemical water-splitting process for co-production of hydrogen and electricity, Int. J. Hydrog. Energy 43 (2018) 17574–17587, https://doi.org/10.1016/j.ijhydene.2018.07.151.

[18] S. Abanades, G. Flamant, Thermochemical hydrogen production from a two-step solar-driven water-splitting cycle based on cerium oxides, Sol. Energy 80 (2006) 1611–1623, https://doi.org/10.1016/j.solener.2005.12.005.
[19] Y. Deng, R. Dewil, L. Appels, S. Li, J. Baeyens, J. Degrève, G. Wang, Thermochemical water splitting: selection of priority reversible redox reactions by multi-attribute decision making, Renew. Energy 170 (2021) 800–810, https://doi.org/10.1016/j.renene.2021.02.009.
[20] C. Agrafiotis, M. Roeb, C. Sattler, A review on solar thermal syngas production via redox pair-based water/carbon dioxide splitting thermochemical cycles, Renew. Sustain. Energy Rev. 42 (2015) 254–285, https://doi.org/10.1016/j.rser.2014.09.039.
[21] A. Le Gal, S. Abanades, Catalytic investigation of ceria-zirconia solid solutions for solar hydrogen production, Int. J. Hydrog. Energy 36 (2011) 4739–4748, https://doi.org/10.1016/j.ijhydene.2011.01.078.
[22] N. Gokon, T. Suda, T. Kodama, Oxygen and hydrogen productivities and repeatable reactivity of 30-mol%-Fe-, Co-, Ni-, Mn-doped $CeO_{2-\delta}$ for thermochemical two-step water-splitting cycle, Energy 90 (2015) 1280–1289, https://doi.org/10.1016/j.energy.2015.06.085.
[23] M. Orfila, D. Sanz, M. Linares, R. Molina, R. Sanz, J. Marugán, J.A. Botas, H_2 production by thermochemical water splitting with reticulated porous structures of ceria-based mixed oxide materials, Int. J. Hydrog. Energy 46 (2021) 17458–17471, https://doi.org/10.1016/j.ijhydene.2020.04.222.
[24] Y. Hao, C.-K. Yang, Haile, M. Sossina, Ceria-zirconia solid solutions ($Ce_{1-x}Zr_xO_{2-y}$, $x < 0.2$) for solar thermochemical water splitting: a thermodynamic study, Chem. Mater. 26 (2014) 6073–6082.
[25] X. Qian, J. He, E. Mastronardo, B. Baldassarri, W. Yuan, C. Wolverton, S.M. Haile, Outstanding properties and performance of $CaTi_{0.5}Mn_{0.5}O_{3-\delta}$ for solar-driven thermochemical hydrogen production, Matter 4 (2021) 688–708, https://doi.org/10.1016/j.matt.2020.11.016.
[26] M.M. Nair, S. Abanades, Experimental screening of perovskite oxides as efficient redox materials for solar thermochemical CO_2 conversion, Sustain. Energy Fuels 2 (2018) 843–854, https://doi.org/10.1039/c7se00516d.
[27] L. Wang, M. Al-Mamun, P. Liu, Y. Wang, H.G. Yang, H. Zhao, Notable hydrogen production on $La_xCa_{1-x}CoO_3$ perovskites via two-step thermochemical water splitting, J. Mater. Sci. 53 (2018) 6796–6806, https://doi.org/10.1007/s10853-018-2004-2.
[28] H. Kaneko, T. Miura, H. Ishihara, S. Taku, T. Yokoyama, H. Nakajima, Y. Tamaura, Reactive ceramics of CeO_2–MO_x (M = Mn, Fe, Ni, Cu) for H_2 generation by two-step water splitting using concentrated solar thermal energy, Energy 32 (2007) 656–663, https://doi.org/10.1016/j.energy.2006.05.002.
[29] T. Kodama, T. Hasegawa, A. Nagasaki, N. Gokon, A reactive Fe-YSZ coated foam device for solar two-step water splitting, J. Sol. Energy Eng. 131 (2009), https://doi.org/10.1115/1.3090819.
[30] J.R. Scheffe, A. Steinfeld, Oxygen exchange materials for solar thermochemical splitting of H_2O and CO_2: a review, Mater. Today 17 (2014) 341–348, https://doi.org/10.1016/j.mattod.2014.04.025.
[31] P. Furler, J. Scheffe, M. Gorbar, L. Moes, U. Vogt, A. Steinfeld, Solar thermochemical CO_2 splitting utilizing a reticulated porous ceria redox system, Energy Fuels 26 (2012) 7051–7059, https://doi.org/10.1021/ef3013757.
[32] D. Marxer, P. Furler, M. Takacs, A. Steinfeld, Solar thermochemical splitting of CO_2 into separate streams of CO and O_2 with high selectivity, stability, conversion, and efficiency, Energy Environ. Sci. (2017), https://doi.org/10.1039/c6ee03776c.
[33] D. Marxer, P. Furler, J. Scheffe, H. Geerlings, C. Falter, V. Batteiger, A. Sizmann, A. Steinfeld, Demonstration of the entire production chain to renewable kerosene via solar thermochemical splitting of H_2O and CO_2, Energy Fuels 29 (2015) 3241–3250, https://doi.org/10.1021/acs.energyfuels.5b00351.
[34] E. Gager, M. Frye, D. McCord, H. Scheffe, J.C. Nino, Reticulated porous lanthanum strontium manganite structures for solar thermochemical hydrogen production, Int. J. Hydrog. Energy 47 (2022) 831152–831162, https://doi.org/10.1016/j.ijhydene.2022.07.052.
[35] A. Haeussler, S. Abanades, A. Julbe, J. Jouannaux, B. Cartoixa, Two-step CO_2 and H_2O splitting using perovskite-coated ceria foam enhanced green fuel production in a porous volumetric solar reactor, J. CO_2 Util. 41 (2020) 101257, https://doi.org/10.1016/j.jcou.2020.101257.
[36] A. Pérez, M. Orfila, M. Linares, R. Sanz, J. Marugán, R. Molina, J.A. Botas, Hydrogen production by thermochemical water splitting with $La_{0.8}Al_{0.2}MeO_{3-\delta}$ (Me = Fe, Co, Ni and Cu) perovskites prepared under controlled pH, Catal. Today 390–391 (2022) 22–33, https://doi.org/10.1016/j.cattod.2021.12.014.
[37] D.R. Barcellos, F.G. Coury, A. Emery, M. Sanders, J. Tong, A. McDaniel, C. Wolverton, M. Kaufman, R. O'Hayre, Phase identification of the layered perovskite $Ce_xSr_{2-x}MnO_4$ and application for solar thermochemical water splitting, Inorg. Chem. 58 (2019) 7705–7714, https://doi.org/10.1021/acs.inorgchem.8b03487.
[38] A. Boretti, Technology readiness level of solar thermochemical splitting cycles, ACS Energy Lett. 6 (2021) 1170–1174, https://doi.org/10.1021/acsenergylett.1c00181.
[39] E. Commission, D.-G. for R and Innovation, Study on 'Solar Fuels Research & Invest: defining and developing the global solar fuel value chain: techno-economic analysis and pathways for sustainable pathways for sustainable implementation', Publ. Off. (2021) https://doi.org/10.2777/508905.
[40] A.M. Huízar-Félix, T. Hernández, S. de la Parra, J. Ibarra, B. Kharisov, Sol-gel based Pechini method synthesis and characterization of $Sm_{1-x}Ca_xFeO_3$ perovskite $0.1 \leq x \leq 0.5$, Powder Technol. 229 (2012) 290–293, https://doi.org/10.1016/j.powtec.2012.06.057.
[41] L. Polonchuk, J. Elbel, L. Eckert, J. Blum, E. Wintermantel, H.M. Eppenberger, Titanium dioxide ceramics control the differentiated phenotype of cardiac muscle cells in culture, Biomaterials (2000), https://doi.org/10.1016/S0142-9612(99)00189-1.
[42] H. Haugen, J. Will, A. Köhler, U. Hopfner, J. Aigner, E. Wintermantel, Ceramic TiO_2-foams: characterisation of a potential scaffold, J. Eur. Ceram. Soc. 24 (2004) 661–668, https://doi.org/10.1016/S0955-2219(03)00255-3.
[43] K. Schwartzwalder, A.W. Somers, Method of Making Porous Ceramic Articles, US Pat 1963, 4.
[44] B. Neumann, T.W. Elkins, W. Dreher, H. Hagelin-Weaver, J.C. Nino, M. Bäumer, Enhanced catalytic methane coupling using novel ceramic foams with bimodal porosity, Catal. Sci. Technol. (2013), https://doi.org/10.1039/c2cy20458d.
[45] H. Giesche, Mercury porosimetry: a general (practical) overview, Part. Part. Syst. Charact. 23 (2006) 9–19, https://doi.org/10.1002/ppsc.200601009.
[46] M. Orfila, M. Linares, R. Molina, J.A. Botas, R. Sanz, J. Marugán, Perovskite materials for hydrogen production by thermochemical water splitting, Int. J. Hydrog. Energy 41 (2016) 19329–19338, https://doi.org/10.1016/j.ijhydene.2016.07.041.
[47] H.P.S. Corrêa, I.P. Cavalcante, D.O. Spuza, E.Z. Santos, M.T.D. Orlando, H. Belich, F.J. Silva, E.F. Medeiro, J.M. PIres, J.L. Passamai, L.G. Martínez, J.L. Rossi, Synthesis and structural characterization of the Ca_2MnReO double perovskite, Ceramica, vol. 56, 2010, pp. 193–200. ⟨https://doi.org/10.1590/s0366-69132010000200015⟩.
[48] I. Ermanoski, J.E. Miller, M.D. Allendorf, Efficiency maximization in solar thermochemical fuel production: challenging the concept of isothermal water splitting, Phys. Chem. Chem. Phys. 16 (2014) 8418–8427, https://doi.org/10.1039/C4CP00978A.
[49] S. Abanades, A. Haeussler, Two-step thermochemical cycles using fibrous ceria pellets for H2 production and CO2 reduction in packed-bed solar reactors, Sustain. Mater. Technol. 29 (2021) e00328, https://doi.org/10.1016/j.susmat.2021.e00328 hal-03365928.